Catalysis Science & Technology

H₂ release

ROYAL SOCIETY
OF CHEMISTRY

PAPER
Moritz Wolf *et al.*
Bimetallic platinum rhenium catalyst for efficient low
temperature dehydrogenation of perhydro benzyltoluene

Check for updates

Bimetallic platinum rhenium catalyst for efficient low temperature dehydrogenation of perhydro benzyltoluene†

Domenic Strauch, [iD] [ab] Pia Weiner,[b] Bidyut Bikash Sarma, [iD] [cd] Andreas Körner, [iD] [ab]
Elisabeth Herzinger,[c] Patrick Wolf,[a] Anna Zimina, [iD] [cd] Andreas Hutzler, [iD] [a]
Dmitry E. Doronkin, [iD] [cd] Jan-Dierk Grunwaldt, [iD] [cd]
Peter Wasserscheid [iD] [ab] and Moritz Wolf [iD] *[ce]

Benzyltoluene (H0-BT) is a promising liquid organic hydrogen carrier (LOHC) molecule. Catalytic hydrogenation of H0-BT to perhydro benzyltoluene (H12-BT) and dehydrogenation back to H0-BT to release the chemically bound hydrogen constitute a suitable and technically relevant hydrogen storage cycle. Herein, we report the development of a bimetallic Pt–Re/Al$_2$O$_3$ catalyst for the dehydrogenation of H12-BT under moderate conditions to enable heat integration of the endothermal dehydrogenation reaction with low temperature waste heat streams. The reducibility of the catalyst is compared to a monometallic Pt/Al$_2$O$_3$ reference system using temperature-programmed reduction (TPR) and *in situ* reduction during X-ray absorption spectroscopy (XAS) to gain insight on the mode of interaction between Pt and Re. TPR and XAS propose full reduction of Pt, while rhenium oxide is only partially reduced at 400 °C. Analysis by means of extended X-ray absorption fine structure suggests a lower coordination number and thus smaller entities of Pt for bimetallic catalysts with increasing Re loading. Further, an electronic modification of Pt is observed, which mostly stems from residual Cl-species from the Pt-precursor, but may also indicate direct interaction with Re. Structural promotion of Pt by Re provided a strong stabilization of smaller clusters and nanoparticles leading to a high Pt dispersion even during catalyst activation in H$_2$ at high temperatures of 700 °C. When compared to the monometallic reference, particularly the initial hydrogen release is accelerated when using Pt–Re/Al$_2$O$_3$ catalysts. Mechanistically, the bimetallic catalysts outperformed the monometallic reference catalyst due to an efficient initial dehydrogenation of H12-BT and a short lifetime of the partially dehydrogenated intermediate (H6-BT) yielding H0-BT as the desired product of the consecutive reaction. The catalytic performance and XAS studies suggest an optimized structural composition of the active Pt phase, potentially *via* an ensemble effect, which allows for efficient H$_2$ release from H12-BT.

Introduction

Hydrogen plays a key role as an energy carrier in establishing renewable, alternative energy sources. However, handling elemental hydrogen remains challenging, especially for the purposes of storage and transportation. Liquid organic hydrogen carriers (LOHCs) offer a promising alternative to existing storage concepts. More than six hundred litres of hydrogen gas at ambient pressure may be chemically bound per litre of LOHC allowing for competitive energy densities when compared to compressed or cryogenic molecular hydrogen. Contrary to the handling of molecular hydrogen, LOHC increases the safety during storage and transportation drastically due to the absence of highly flammable molecular hydrogen. In addition, storage and logistics of LOHCs are possible in existing fuel tanks or tankers and are associated with minimal loss and energy consumption due to the liquid nature of the carrier molecules and the chemical bonding of the hydrogen. Optimized catalysts are required, though, to enable efficient storage cycles *via* reversible loading through catalytic hydrogenation and catalytic dehydrogenation.[1,2]

[a] *Helmholtz Institute Erlangen-Nürnberg for Renewable Energy (IEK-11), Forschungszentrum Jülich GmbH, Cauerstr. 1, 91058 Erlangen, Germany*

[b] *Lehrstuhl für Chemische Reaktionstechnik (CRT), Friedrich-Alexander-Universität Erlangen-Nürnberg (FAU), Egerlandstr. 3, 91058 Erlangen, Germany*

[c] *Institute of Catalysis Research and Technology (KIT), Hermann-von-Helmholtz-Platz 1, 76344 Eggenstein-Leopoldshafen, Germany. E-mail: moritz.wolf@kit.edu*

[d] *Institute for Chemical Technology and Polymer Chemistry, Karlsruhe Institute of Technology (KIT), Engesserstr. 20, 76131 Karlsruhe, Germany*

[e] *Engler-Bunte-Institut, Karlsruhe Institute of Technology (KIT), Engler-Bunte-Ring 1, 76131 Karlsruhe, Germany*

† Electronic supplementary information (ESI) available. See DOI: https://doi.org/10.1039/d3cy01336g

This journal is © The Royal Society of Chemistry 2024

Catal. Sci. Technol., 2024, **14**, 1775–1790 | 1775

Benzyltoluene (H0-BT) is a commercial heat transfer fluid with the tradename Marlotherm® LH and composed of a mixture of three structural isomers with the methyl group on one of the aromatic rings in *ortho*, *meta*, or *para* orientation.[3,4] Full hydrogenation of H0-BT to perhydro benzyltoluene (H12-BT) may chemically bind 12 hydrogen atoms. The thermodynamically most stable intermediates in the hydrogenation and dehydrogenation processes are partially hydrogenated benzyltoluene species (H6-BT) with one aromatic ring.[3,5,6] The LOHC system H0-BT/H12-BT has a high hydrogen storage capacity of 6.2 wt%, provides a high thermal stability of the LOHC molecule, and enables a facile gas–liquid separation due to the high boiling points of the involved LOHC compounds allowing for an excellent purity of hydrogen.[3] In the first commercialization examples of perhydro benzyltoluene dehydrogenation, a sulphur modified Pt/Al$_2$O$_3$ core shell catalyst is used.[7–11]

In order to develop more efficient dehydrogenation catalysts for the LOHC technology, we explore bimetallic catalyst systems in this contribution. In this context, well-known catalysts from petrochemical and refinery processes[11–15] represent a good starting point. For example, a team of the Chevron Research Company patented in 1968 a Pt–Re/Al$_2$O$_3$ system for the catalytic reforming process of sulphur-free naphtha.[12] With the establishment of bimetallic Pt–Re systems in catalytic reforming, similar catalysts were also applied in the gas phase dehydrogenation of methylcyclohexane to toluene. In this respect, various research groups demonstrated a similar or even reduced dehydrogenation activity when compared to monometallic platinum catalysts.[13–17] Contrary, van Trimpont *et al.* investigated kinetic effects of Re in bimetallic Pt–Re/Al$_2$O$_3$ catalysts.[14] For a monometallic Pt/Al$_2$O$_3$ catalyst, the reaction rate decreased with increasing partial pressure of hydrogen, while the rate remained constant for the platinum–rhenium system.[14] In general, literature mostly ascribes the major benefits of Re (typically in combination with sulphur modification) to a suppressed coke formation[18] and a physical stabilization of the active Pt phase.[12,19] For example, an increased thermal stability of Pt against sintering at elevated temperatures has been observed for bimetallic Pt–Re systems.[20] Yermakov *et al.* attribute this property to the strong bond between rhenium and alumina, which maintains a high platinum dispersion through interaction with platinum.[20] Opposing conclusions on the influence of rhenium in Pt–Re catalysts are reported for reaction kinetics, which has been summarized by Alhumaidan *et al.*[21]

The development of efficient and stable catalysts for hydrogen release from LOHC systems is crucial to meet the economic and ecological demands of this upcoming hydrogen storage technology. In detail, we study the influence of rhenium promotion on the active platinum phase in the dehydrogenation of H12-BT. Pt–Re/Al$_2$O$_3$ catalysts with various compositions are prepared *via* wet impregnation and compared to monometallic Pt/Al$_2$O$_3$ catalysts. Conventional characterization techniques as well as *in situ* X-ray absorption spectroscopy are employed to identify structural and electronic effects induced by the presence of rhenium in the catalyst material.

Methodology

Chloroplatinic acid (Pt content ≥37.5 mol%), rhenium(VII) oxide (Re content ≥76.5 mol%), ethanol (purity ≥99.8%), and isopropanol (purity ≥99.9%) were purchased from Sigma Aldrich. These chemicals were used as received. Benzyltoluene (H0-BT, Marlotherm® LH) was purchased from Eastman Chemical Company (Marlotherm LH) and hydrogenated at 300 °C and 30 bar H$_2$ using a commercial Pt–Pd/Al$_2$O$_3$ catalyst (EleMax H, Clariant Produkte GmbH, Germany) in a trickle bed reactor set-up yielding a final purity of >99.4% H12-BT with minor impurities of partially hydrogenated benzyl toluene (H6-BT). Boehmite (PURAL TH300) was purchased from Sasol Germany and heated to 550 °C for 3 h in a muffle furnace under ambient atmosphere to yield the alumina support.

The catalysts were prepared *via* wet impregnation with ion adsorption. A precursor solution was prepared using ultrapure water and an appropriate amount of H$_2$[PtCl$_6$] as well as Re$_2$O$_7$. A molarity of 3.08×10^{-2} mmol L^{-1} (0.05 wt% platinum) was targeted, which results in a pH of 2–3. Subsequently, the calculated amount of alumina was added immediately to the as-prepared impregnation solution targeting a Pt loading of 0.3 wt% and Re loadings of 0, 0.03, 0.15, 0.30, or 0.90 wt%. The resulting dispersion was stirred for 10 min. The dispersion was then transferred to a rotary evaporator at 50 °C to remove the water solvent. A drying sequence with a total duration of 3 h and four subsequent steps between 140 and 20 mbar was then applied (Table S1 in ESI†) to evaporate all water to dryness under low pressure. Calcination of the dried catalyst was conducted in a Nabertherm L9/11 muffle furnace at 400 °C for 4 h under a flow of 300 mL min^{-1} air with a heating ramp of 10 °C min^{-1}.

The metal loadings of the catalysts were determined by means of atomic emission spectrometry (Ciros CCD, Spectro Analytical Instruments GmbH) with inductively coupled plasma (ICP-AES). For this purpose, 200 mg of catalyst were dissolved in 100 mL HCl–HNO$_3$ mixture with a molar ratio of 3:2 using a microwave. The concentrations of platinum and rhenium in the solution were calculated by the characteristic wavelength at 214.423 and 221.416 nm, respectively. Morphological analysis of the calcined alumina support was carried out by means of physisorption at −196 °C in a Quantasorb SI (Quantachrome Instruments). At first, about 300 mg of the sample was degassed by heating to 250 °C under vacuum for 12 h. The specific surface area was determined by N$_2$ physisorption in the pressure range of 0.05–0.3 p p_0^{-1} with subsequent analysis by the BET method, while the pore size distribution was determined using the BJH method on the adsorption and desorption branches of the isotherm. To determine the point of zero charge (PZC) of the metal oxide support, the salt addition method was

1776 | *Catal. Sci. Technol.*, 2024, **14**, 1775–1790

This journal is © The Royal Society of Chemistry 2024

employed.[22,23] Identical proportions of the sample were added to a series of solutions with the same ionic strength, but varying pH. A certain change in pH is observed upon addition of the sample to the solutions. Aqueous solutions with pH values ranging from 3 to 10 ($\pm$0.1) were prepared using 0.1 M $NaNO_3$ mixed with 0.1 M HNO_3 and 0.1 M NaOH. Subsequently, 0.05 g of solid sample was added to 10 g of each solution with various pH values (pH_i). Following this, the samples were mixed on a shaking plate (VWR, Thermal Shake Lite) for 24 h at 300 rpm and 25 °C. After filtration of the solids, the pH of the sample solution was measured yielding pH_f. The change of pH value (ΔpH) is obtained by the difference between pH_i and pH_f. The pH at PZC (pH_{PZC}) is represented by the intersection with the abscissa in a ΔpH–pH_i plot. X-ray diffraction (XRD) was conducted with an X'Pert Pro MPD (Panalytical) in Bragg–Brentano geometry using a copper X-ray source ($\lambda_{K\alpha}$ = 1.5406 Å). The patterns were acquired from 13–80° 2θ with a step size of 0.016711° and an acquisition time of 0.2 s. Temperature-programmed reduction (TPR) was conducted in an Autochem II (Micromeritics). For this purpose, a total of 377 mg of catalyst was loaded and heated to 400 °C with 10 °C min^{-1} in pure oxygen with a holding time of 60 min. The catalyst was then cooled to 50 °C and TPR was initiated with a temperature ramp of 10 °C min^{-1} and a flow of 10% H_2 in 20 mL min^{-1} argon. H_2 consumption peaks were deconvoluted, integrated, and normalized to the initial sample weight. The ratio of the H_2 consumption over the expected consumption from the reduction of metal oxides provides the degree of reduction (DOR). High-angle annular dark field scanning transmission electron microscopy (HAADF-STEM) was employed for the analysis of nanoparticles in the catalysts, also in combination with energy-dispersive X-ray (STEM-EDX) spectroscopy. The work was carried out using a Talos F200i (ThermoFisher Scientific) and an ARM200F (JEOL) with an acceleration voltage of 30–200 kV. Remote air plasma cleaning was performed when necessary, using a Tergeo-EM plasma cleaner (PIE Scientific) to remove adsorbed hydrocarbons mitigating carbon deposition during imaging. Spectrum images were visualized using AZtecTEM and Velox. Cluster sizes were analysed by measuring the diameter of at least 120 clusters larger >0.4 nm using ImageJ.[24]

In situ XAS in terms of X-ray absorption near edge structure (XANES) and extended X-ray absorption fine structure (EXAFS) was conducted at PETRA III synchrotron radiation source (DESY, Hamburg, Germany), beamline P65. The energy of the X-ray photons was selected by a Si(111) double-crystal monochromator and the beam size was set by means of slits to 0.3 (vertical) × 1.5 (horizontal) mm^2. An energy dispersive detector (Hitachi Vortex-ME4 with 2 mm element thickness) was used to collect the fluorescence X-rays. Re L_3 and Pt L_3 edges were recorded in parallel in a single scan. An additional ionization chamber I_2 behind the sample detectors (I_0 and I_1) was used to record a spectrum of Pt foil required for precise energy calibration. The Pt L_3 (11

564 eV) and Re L_3 (10 535 eV) edges were monitored during TPR of the calcined catalysts from 25 to 400 °C min in 11% H_2/He (30 mL min^{-1}) using a heating rate of 10 °C min^{-1} and a 30 min holding time at 400 °C. Pressed and sieved catalysts (0.1–0.2 mm sieve fraction) were placed in quartz capillaries (1.5 mm outer diameter, 0.02 mm wall thickness) between quartz wool plugs. XAS data reduction was carried out using the standard Demeter software package.[25] Data reduction (alignment and normalization) was performed using Athena (version 0.9.26). Energy scale was calibrated to the position of the maximum of the first derivative in the spectrum of Pt foil reference. All experimental spectra were then aligned to the reference by using Pt foil data from the corresponding reference channels. Linear combination analysis (LCA) of XANES spectra was performed using the first and the last spectra recorded during TPR as internal references. First shell EXAFS refinement was performed on spectra measured after TPRs using Artemis (version 0.8.012) in R-space (k-range from 2 to 9 $Å^{-1}$, limited by the overlap with Re L_3 edge, R-range 1–3 Å). Amplitude reduction factor determined from a fit of Pt foil reference measurement was 0.67. Coordination numbers (CN), interatomic distances (r), energy shift (δ_{E0}) and mean square deviation of interatomic distances (σ^2) were refined during fitting. The absolute misfit between theory and experiment was expressed by ρ.[25]

Catalyst activation, that is reduction of the oxidic platinum phase, was carried out by means of thermal reduction in a Carbolite horizontal tube furnace (Gero type). The catalyst was loaded into a ceramic boat, which was placed in a quartz glass tube (ID: 42 mm, L: 550 mm). The reduction was initiated by replacing 50 mL min^{-1} of N_2 by H_2 after heating up with 10 °C min^{-1} under a flow of 500 mL min^{-1} N_2 and stabilization of the reduction temperature at 400 °C. Alternatively, the catalysts were reduced at 250 or 700 °C. After reduction for 120 min, the catalyst was exposed to a flow of N_2 during cool-down.

Dehydrogenation experiments were carried out in a semi-batch mode using a 100 mL five-neck round-bottom flask (Fig. S1†). The glass flask was placed in a heating mantle (Winkler AG, Germany) on a magnetic stirrer. A Teflon-coated stirring bar was placed in the flask before the start of the experiment to ensure mixing. A mass flow controller (Bronkhorst) allows for gas dosing and inertisation of the reaction chamber with Ar *via* one of the side necks. A catalyst addition apparatus made of stainless steel in another neck enables addition of the catalyst under reaction conditions. The central neck is connected to a reflux condenser cooled to 3 °C to condensate evaporated LOHC and other condensable species. A Pt-100 probe is monitoring the temperature in the liquid phase and the last neck is used for sampling liquids during the experiment. The LOHC equivalent of 2 g of reversibly bound H_2 (32.25 g H12-BT) was loaded into the flask. The molar ratio of Pt:LOHC was 1:10 000 for all experiments. The corresponding amount of catalyst was loaded into the catalyst addition apparatus. The set-up was inertised with Ar and the flask was heated to the desired

Paper

reaction temperature of typically 250 °C. The reaction temperature was only altered to 240, 230, 220, or 210 °C for the kinetic studies. Optionally, a continuous flow of 200 mL min^{-1} argon served as a carrier gas for the released hydrogen during the whole experiment. The catalyst was added to initiate the dehydrogenation experiment once the temperature stabilized. The general run time was 240 min under ambient pressure. A total of 0.1 mL was sampled via a syringe after 0, 30, 60, 120, and 240 min for detailed analysis of the composition of the liquid phase. For analysis of side product formation, another sample was acquired after 1320 min during a long-term experiment. In case of Ar overflow, the hydrogen concentration in the off-gas was continuously monitored using a thermal conductivity detector (TCD, FTC 300, Messkonzept GmbH).

The volume of released H_2 (V_{H_2}) was calculated based on its fraction in the gas phase y_{H_2} obtained via the TCD with a resolution of $\Delta t = 1$ s and can be determined using eqn (1).

$$V_{H_2} = \frac{y_{H_2} \cdot \frac{\dot{V}_{Ar}}{60} \cdot \Delta t}{1 - y_{H_2}} + \sum_{t_0}^{t-1} V_{H_2} \qquad (1)$$

where $\dot{V}_{Ar}$ is the set volumetric flow of Ar (200 mL min^{-1}).

The resulting degree of dehydrogenation (DoDH) is calculated using eqn (2) and acts as a descriptor of the overall release of H_2 during the sequential dehydrogenation of H12-BT to H0-BT via H6-BT.[3,26]

$$DoDH_{TCD} = \frac{V_{H_2}}{V_{H_2,\,max}} \qquad (2)$$

where $V_{H_2,max}$ is the maximum volume of reversibly bound hydrogen, namely 2 g corresponding to 24.27 L of H_2 under standard conditions, in the H12-BT and the subscript TCD indicates the analysis method.

The productivity of Pt in the catalysts with respect to released H_2 during a time interval Δt was determined using eqn (3).

$$\text{Productivity} = \frac{m_{H_2}}{m_{Pt} \cdot \Delta t} \qquad (3)$$

where m_{Pt} corresponds to the mass of platinum in the loaded catalyst.

The composition of liquid samples was analysed by means of gas chromatography with a flame ionization detector (GC-FID) to directly determine the DoDH in the liquid phase and to evaluate the formation of methylfluorene species. A Trace 1310 (Fisher Scientific) equipped with a Rxi17Sil column with a length of 30 m was applied. Two separate analyses were conducted with 30 mg of the liquid sample in 700 mg isopropanol. The LOHC species were quantified by the peak area fraction in the chromatograms to calculate their fraction in the mixture and ultimately the degree of hydrogenation (DoH, eqn (4)), while the degree of dehydrogenation was calculated using eqn (5).

$$DoH_{GC} \text{ in } \% = 100 \cdot [x_{H12\text{-}BT} + 0.5 \cdot x_{H6\text{-}BT}] \qquad (4)$$

$$DoDH_{GC} \text{ in } \% = 100 - DoH \qquad (5)$$

where x_i corresponds to the peak area of species i relative to the total peak area of the chromatograms and the subscript GC indicates the analysis method.

Results and discussion

At first, the physico-chemical properties of the Al_2O_3 support were determined after calcination of the boehmite precursor. Analysis by means of N_2 physisorption (Fig. S2 in ESI†) resulted in a BET surface area of 89 m^2 g^{-1} while BJH analysis suggests an average pore size of 38 nm. A PZC of 6.5 was obtained for the as-prepared catalyst support (Fig. S3†). Hence, a good interaction of the support with the $[PtCl_6]^{2-}$ anions of the Pt precursor is expected via ion adsorption as the pH during impregnation of 2–3 is lower than the PZC. XRD analysis of the calcined boehmite precursor confirmed the formation of γ-Al_2O_3 (Fig. S4†). Pt as the active species and Re as promotor were added via wet impregnation of the Al_2O_3 support followed by calcination in air.

The as-prepared catalysts were analysed by means of elemental analysis using ICP-AES, which confirmed the targeted Pt loading of 0.3 wt% and the coexistence of Pt and Re with various gravimetric Pt : Re ratios ranging from 1 : 0 (monometallic Pt) to 1 : 3 (Table 1). In addition, a monometallic Re/Al_2O_3 reference catalyst was prepared. All catalysts were analysed by means of STEM, but

Table 1 Metal loadings and resulting gravimetric Pt : Re ratio from analysis by means of ICP-AES of the catalysts as well as average size of the platinum and rhenium oxide clusters

Catalyst	Pt loading/wt%	Re loading/wt%	Mass ratio Pt : Re/—	d_{metal}[a]/nm
Pt–Re 1 : 0	0.31	—	1 : 0	1.07
Pt–Re 1 : 0.1	0.29	0.03	1 : 0.10	n/a
Pt–Re 1 : 0.5	0.29	0.14	1 : 0.48	1.06
Pt–Re 1 : 1	0.29	0.29	1 : 1.00	n/a
Pt–Re 1 : 3	0.29	0.88	1 : 3.05	n/a
Pt–Re 0 : 1	—	0.3	0 : 1	1.05

[a] With the applied microscopic techniques, we cannot distinguish between Pt and Re nanoparticles in the case of bimetallic catalysts due to the low loadings. There d_{metal} gives the result of the HRSTEM analysis without distinguishing between the two elements and ignoring clusters smaller than 0.5 nm in diameter.
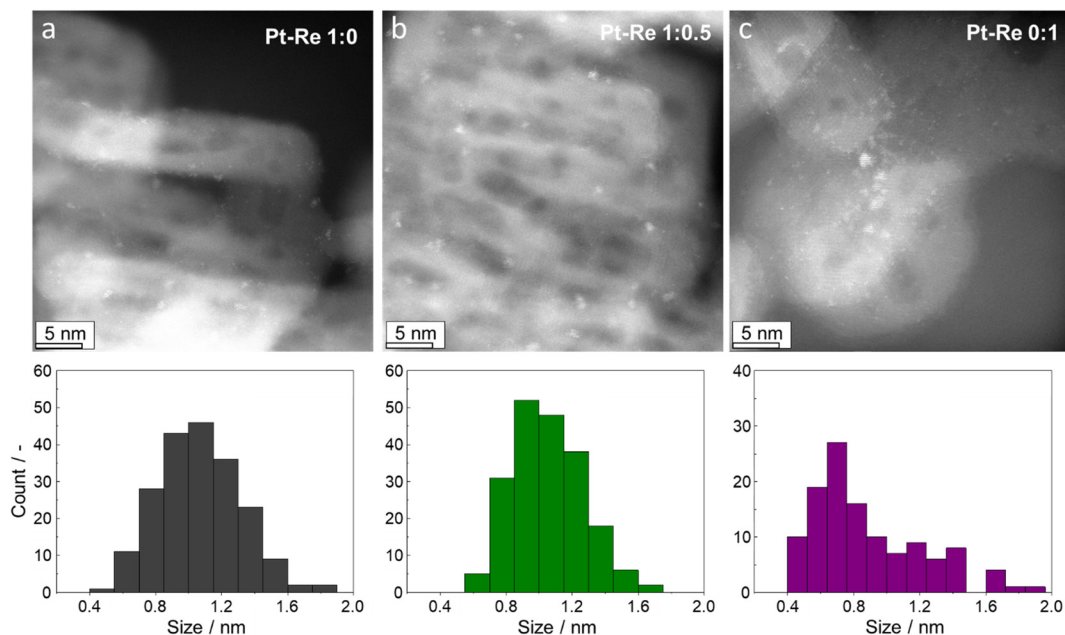
Fig. 1 High-angle annular dark field scanning transmission electron micrographs of (a) the monometallic Pt–Re 1 : 0, (b) the bimetallic Pt–Re 1 : 0.5, and (c) the reference sample Pt–Re 0 : 1 with histograms of the size distribution. Note, that only clusters >0.4 nm were measured.

differentiation between Pt and Re with common techniques, such as energy-dispersive X-ray spectroscopy (STEM-EDX, Fig. S5†), is challenging due to the large required electron dose for spectrum imaging and the low stability of Pt/Re clusters under irradiation (beam damage). Moreover, carbon deposition, charging of the Al_2O_3 support, similar atomic numbers of Pt (78) and Re (75), and the low metal loading further complicate a clear discrimination between Pt and Re. Hence, bimetallic catalysts were compared with the monometallic reference catalysts, which may allow for indirect differentiation of the noble metal fractions. Nevertheless, STEM analysis resulted in similar observations for all analysed catalysts. Nanoparticles below 2 nm, clusters,

and even single-atoms were identified for both monometallic Pt/Al_2O_3 and Re/Al_2O_3 references as well as for a bimetallic $Pt–Re/Al_2O_3$ catalysts with a gravimetric ratio of 1 : 0.5 (Fig. 1). The size of identified clusters and nanoparticles, which consequently can only be obtained for both metals together, lies within the range of 0.6–1.7 nm.

TPRs of the calcined catalysts with various Pt : Re ratios suggest drastic changes in the overall reduction behaviour when the monometallic references are compared with the bimetallic catalysts (Fig. 2). The previously reported two-step reduction with H_2 consumption peaks at ~220 °C and at elevated temperatures in the range of 350 to 450 °C (ref. 27–33) is observed for all bimetallic catalysts. The H_2 consumption of the monometallic Pt–Re 1 : 0 corresponds well with the expected consumption for full reduction (Table 2). With increasing Re loading, the integral H_2
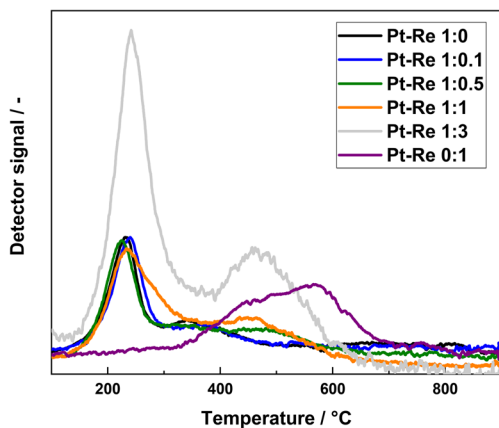

Fig. 2 Temperature-programmed reduction of as-prepared bimetallic Pt–Re/Al_2O_3 catalysts and the monometallic references. Analysis parameters: 10% H_2/Ar, 10 °C min⁻¹.

Table 2 Hydrogen consumption and global degree of reduction when reaching 400 °C and after temperature-programmed reduction

Catalyst	H_2 consumption/μmol g_{cat}^{-1}		DOR[a]/%	
	400 °C	Final	400 °C	Final
Pt–Re 1 : 0	56.3	61.7	92.0	100.7
Pt–Re 1 : 0.1	66.6	86.0	67.4	87.0
Pt–Re 1 : 0.5	72.9	106.6	61.9	90.6
Pt–Re 1 : 1	88.0	137.1	50.5	78.7
Pt–Re 1 : 3	190.1	253.2	47.6	63.4
Pt–Re 0 : 1	14.8	104.6	13.1	92.8

[a] Based on H_2 consumption during TPR and total amount of Pt and Re in catalyst according to ICP-AES.

consumption increases as well for the bimetallic catalysts. As the combined H_2 consumption at 400 °C is lower for the reference catalysts Pt–Re 1:0 and Pt–Re 0:1 than for the one of Pt–Re 1:1 (Table 2) with equal amounts of metal loadings, the correlation between Re content and H_2 consumption is not only linked to the increased loadings of reducible metal oxides, but also related to the Pt-assisted reduction of the Re phase. Assuming complete reduction of Pt with similar reduction behaviour as for the monometallic reference, a reduction of rhenium oxide may be observed at lower temperatures. However, a smaller fraction of rhenium oxide is reduced with increasing Re content as suggested by the integral H_2 consumption (Table 2). Even though the expected close vicinity of Pt and Re species enables hydrogen spillover,[31,34] only a partial reduction of the rhenium oxide phase is expected, particularly for higher Re loadings and at

the herein selected reduction temperature of 400 °C. Nevertheless, the reduction behaviour of bimetallic Pt–Re/Al_2O_3 catalysts suggests significant interactions between the two metals.[27–33] The mode of Pt-assisted reduction of rhenium oxide phases in the Pt–Re/Al_2O_3 catalysts changes from low Re loadings to Pt–Re 1:1 and in particular for Pt–Re 1:3. For the latter, TPR exhibits a significant contribution of the reduction of rhenium oxide to the detected H_2 consumption at 220 °C (Fig. 2). Here, a shoulder is observed for Pt–Re 1:1, while all other Pt containing catalysts result in a similar TPR profile below 400 °C.

Analysis of the catalysts in the activated state and during reduction by means of *in situ* XAS may provide insight into the extent of physical or chemical promotion of Pt by rhenium, *e.g. via* the ensemble effect[35] or electronic modification[36] of Pt, respectively. Further, EXAFS represents
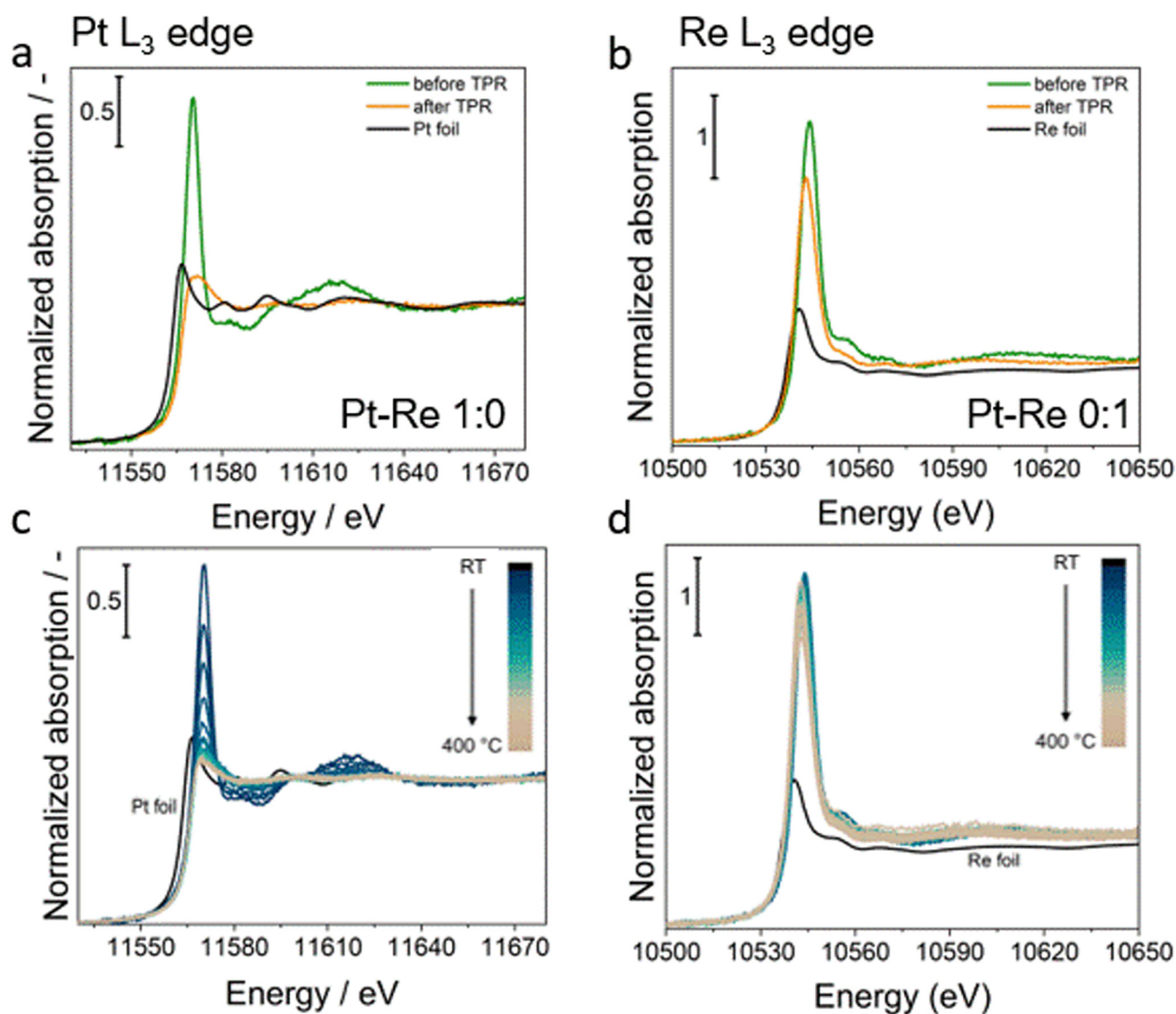

Fig. 3 Comparison of *in situ* X-ray absorption near edge spectra at the Pt and Re L₃ edge acquired at room temperature before and after reduction of (a) the monometallic Pt–Re 1:0 and (b) Pt–Re 0:1 reference catalysts in 11% H_2/He together with a spectrum for Pt foil, as well as (c and d) *in situ* spectra during reduction at 400 °C for 30 min with 10 °C min⁻¹.

1780 | *Catal. Sci. Technol.*, 2024, **14**, 1775–1790

This journal is © The Royal Society of Chemistry 2024

one of the few characterization methods to compare average Pt nanoparticle sizes as classical techniques, such as CO chemisorption and STEM may not be applied for selective size analysis of Pt in the herein studied bimetallic catalysts. The catalysts were reduced in H_2 in a capillary reactor at the P65 beamline at DESY.[37,38] At first, the monometallic Pt/Al_2O_3 and Re/Al_2O_3 references were analysed at the Pt and Re L_3 edge. In the calcined state, Pt–Re 1:0 displays a comparable spectrum to reported XANES analyses of Pt/Al_2O_3 catalysts with an absorption edge energy of 11 564.7 eV (Fig. 3a).[30,39] The white line intensity suggests an initial oxidation state of Pt^{2+}, while rapid reduction to Pt^0 is observed during TPR (Fig. 3c).[40,41] Already the first spectra at 60 °C show a significant degree of reduction, while mostly metallic platinum is expected at 150 °C. Therefore, complete reduction can be expected at 400 °C, which has already been suggested by TPR (Fig. 2). A significant shift of the absorption edge energy of 11 570.1 eV is observed for the Pt–Re 1:0 catalyst when compared to the one of Pt foil (11 564.0 eV). Such a drastic shift is typically only observed for strongly interacting species on the Pt surface and may be linked to platinum chloride species, such as $PtCl_2$ or $PtCl_4$.[42,43] Since hexachloroplatinic acid was used as Pt precursor for all catalysts and chlorine is not expected to be completely removed during catalyst preparation, residual chloride species on the surface of Pt after reduction in H_2 are likely.[44,45] This observation must be considered during evaluation of the catalytic performance. Aside from the shift of the absorption edge energy, the XANES region also strongly differs from the Pt foil, which might be linked to size effects when comparing Pt cluster with the macroscopic Pt foil or may be another artefact from platinum-chloride

complexes in combination with platinum–support interaction.[46]

The *in situ* XANES analysis of the Pt–Re 0:1 reference exhibits the difficult-to-reduce character of Al_2O_3-supported Re_2O_7 (Fig. 3b and d), as observed during TPR (Fig. 2). Here, strong interaction with alumina have been reported to even further suppress reduction.[47] The white line intensity is only slightly reduced, while this observation was mostly limited to the holding time at 400 °C (Fig. 3d). Hence, only a minor degree of reduction is expected with an absorption edge energy shift from 10 541.5 to 10 540.5 eV and the monometallic Re/Al_2O_3 reference catalyst mostly remains in the initial oxidation state of Re(VII).

Detailed *in situ* XANES results for the bimetallic Pt–Re/Al_2O_3 catalysts are summarized in the ESI† (Fig. S6†) and accompanied by LCA (Fig. S7†), which confirm the promotional effect of Pt on the reduction behaviour of Re as evidenced during TPR (Fig. 2). Further, comparison of the spectra at the Pt L_3 edge after reduction shows a clearly increased intensity of the white line and a slight shift to lower absorption energies for Pt with increasing Re loading (Fig. 4a). Both observations indicate an increasing deviation of the electronic properties of Pt when compared to the monometallic Pt/Al_2O_3 reference. X-ray photoelectron spectroscopy (XPS) may provide further insight, but is not feasible with the low loadings in the herein studied catalysts. The shift of the absorption edge may also indicate enhanced removal of Cl-species with increased Re loading. The spectra at the Re L_3 edge indicate a slightly increasing degree of reduction of rhenium with increasing Re loading (Fig. 4b), which may be linked to more efficient Pt-assisted reduction due to a higher degree of interaction as indicated by TPR
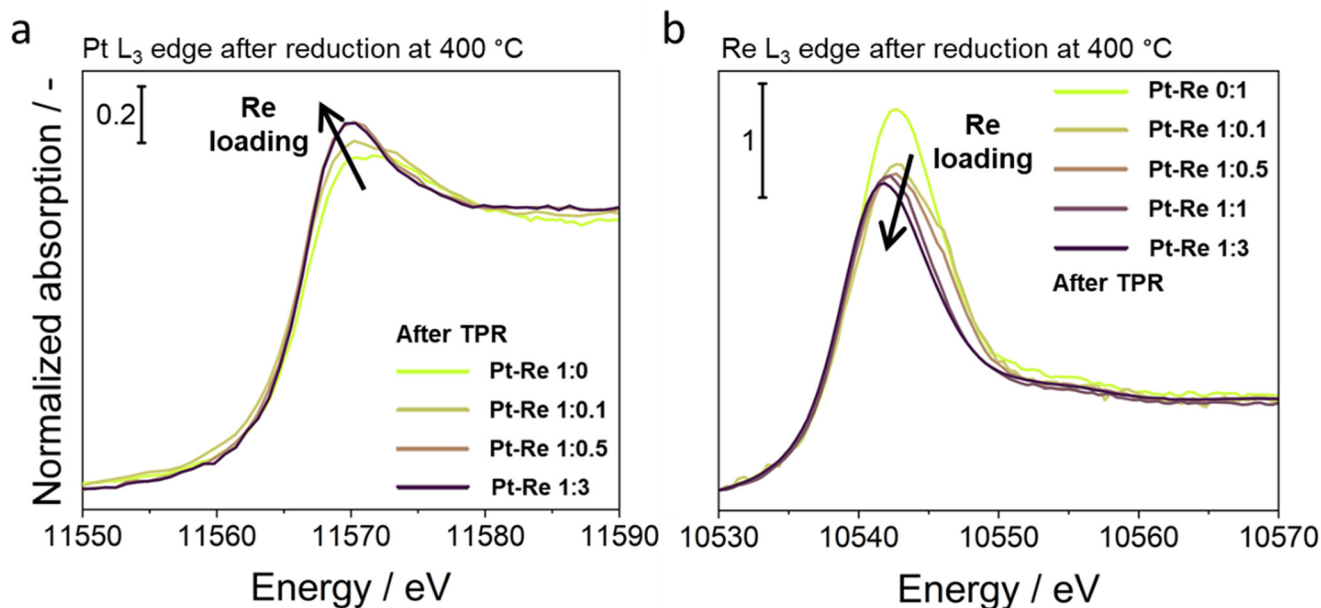

Fig. 4 Comparison of *in situ* X-ray absorption spectra at (a) the Pt and (b) Re L_3 edge after reduction of the bimetallic Pt–Re catalysts with various ratios at 400 °C for 30 min with 10 °C min^{-1} in 11% H_2/He. Spectra were acquired after cool-down to room temperature in 11% H_2/He.

This journal is © The Royal Society of Chemistry 2024

Catal. Sci. Technol., 2024, **14**, 1775–1790 | 1781

(Fig. 2). However, the maximum difference in the oxidation state of Re is observed between the Pt–Re 0:1 reference and the bimetallic catalysts. Noteworthy, the generally expected decrease in peak intensity and shift to a lower absorption energy for reduction from Re(VII) to Re(VI) or Re(IV) are rather small as shown by several groups.[48,49]

EXAFS analysis of the obtained data may provide more information on the local coordination of Pt even though the Re L_3 edge limits the k-range available for analysis of the Pt L_3 edge. The EXAFS spectra of the Pt L_3 edge of bimetallic catalysts are quite consistent amongst each other (Fig. 5, S8 and S9†). Thus, comparable coordination of Pt can be expected for the Pt–Re/Al$_2$O$_3$ catalysts. The previously identified changes of the white line intensity and absorption energy (Fig. 4a) also result in a deviation of the Fourier transforms of the EXAFS data when comparing the bimetallic catalysts with the Pt–Re 1:0 reference and particularly Pt foil. The electronic properties of Pt are seemingly altered with different loading of Re in Pt–Re/Al$_2$O$_3$ catalysts, either by facilitating removal of residual Cl-species or direct electronic interaction. Further, possible interaction may exist with alumina. Since effects from strong metal–support interaction (SMSI) are typically exclusively observed for reducible supports and EXAFS does not hint towards significant backscattering by Al neighbouring atoms, a certain influence is also attributed to the adsorption of residual chloride complexes after reduction in H$_2$.[50] Analysis of the first Pt shell suggests constant Pt–Pt/Re distances and a decreased Pt coordination number for the highest Re loadings (Table 3). In particular, Pt–Re 1:3 has a low CN suggesting a highly dispersed noble metal phase. The resulting decrease in Pt cluster size with increasing Re loading thus points towards an increase in the dispersion of Pt, which has been reported for Pt–Re catalysts.[20] This may become highly relevant during dehydrogenation of H12-BT. For example, Auer *et al.* described a structural dependency and desorption as rate limiting step that may suppress efficient dehydrogenation of perhydro dibenzyltoluene (H18-DBT), which is a related LOHC with similar physical and chemical properties to H12-BT.[8]

The prepared and reduced catalysts were tested in the H$_2$ release from H12-BT (catalytic H12-BT dehydrogenation) in a semi-batch set-up at ambient pressure and 250 °C, where the amount of LOHC in the reaction vessel remained constant. At first, no additional gas flow is used. As the dehydrogenation yields H0-BT in a consecutive reaction via H6-BT isomers as intermediates,[3] the overall conversion of H12-BT is represented by the degree of dehydrogenation (DoDH) to also account for the partial dehydrogenation to H6-BT. Aside from Pt–Re 1:3, all bimetallic catalysts outperformed the monometallic Pt–Re 1:0 reference catalyst (Fig. 6a). The presence of Re particularly accelerated the initial H$_2$ release below DoDHs of 40%. In fact, even the Pt–Re 1:3 catalyst resulted in a higher DoDH in the first liquid sample after 30 min. A gravimetric Pt:Re ratio of 1:0.5 resulted in the highest DoDH for all liquid samples
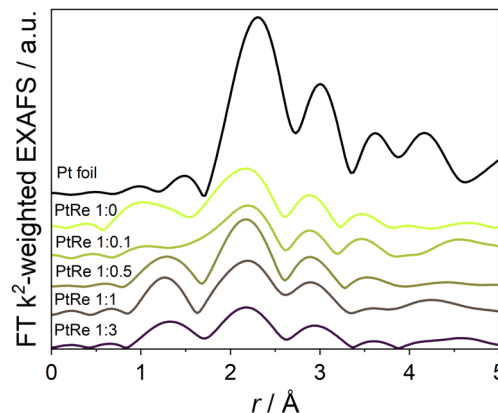

Fig. 5 Fourier-transformed EXAFS spectra (Pt L_3 edge, k^2-weighted) of the bimetallic Pt–Re catalysts with various ratios after reduction at 400 °C for 30 min with 10 °C min^{-1} in 11% H$_2$/He. Spectra were acquired after cool-down to room temperature in 11% H$_2$/He.

suggesting an optimum catalyst composition for Pt–Re 1:0.5. In general, the high initial activity of bimetallic catalysts and the good performance of the herein studied catalysts suggests a negligible poisoning effect of Pt by interaction with chloride species from the catalyst preparation as unravelled by XANES (Fig. 3). A similar DoDH of ∼80% was obtained for all catalysts after 1320 min as the thermodynamic driving force for further dehydrogenation is a limiting factor under the applied conditions.[3] However, the Pt–Re 1:3 catalyst only resulted in a DoDH of 62%.

Methylfluorene species are the most common side products during dehydrogenation of H12-BT.[3] Their formation represents a dehydrocyclisation step, that is a consecutive "deep" dehydrogenation of H0-BT releasing an additional molecule of H$_2$ (Fig. 7). Hence, the production of this side product is directly linked to the concentration of H0-BT and the undesired selectivity of the catalysts to methylfluorene must be compared to the concentration of H0-BT to ensure a fair comparison of different catalyst materials (Fig. 6b). All Pt–Re ratios result in a comparable initial formation of methylfluorene species below 2.1%, while the most active bimetallic catalysts produce significantly higher amounts during the long-term exposure with concentrations of 5.0–7.5%. This observation is seemingly linked to the generally accelerated dehydrogenation of H12-BT, which potentially also favours "deep" dehydrogenation with the formation of methylfluorene species. In general, low coordinated Pt atoms are typically the major cause of side product formation in the dehydrogenation of aromatic and heteroatom-free LOHCs.[51] As clusters and even single atoms were observed for all catalysts, these sites may contribute significantly to the observed formation of methylfluorene species.[51] Regarding the suitability of H12-BT as LOHC, Rüde *et al.* observed an accumulation of less than 1.5% methylfluorene species after several loading and unloading cycles at 290 °C using a commercial, selectively poisoned catalyst.[3] Hence, selective poisoning with sulphur species is also applicable for the dehydrogenation of H12-BT and

1782 | *Catal. Sci. Technol.*, 2024, **14**, 1775–1790

This journal is © The Royal Society of Chemistry 2024

Table 3 Extended X-ray absorption fine structure analysis of the atomic distances and coordination numbers in various catalysts after reduction at 400 °C for 30 min with 10 °C min^{-1} in 11% H$_2$/He. Note that Pt and Re scatterers are indistinguishable in EXAFS

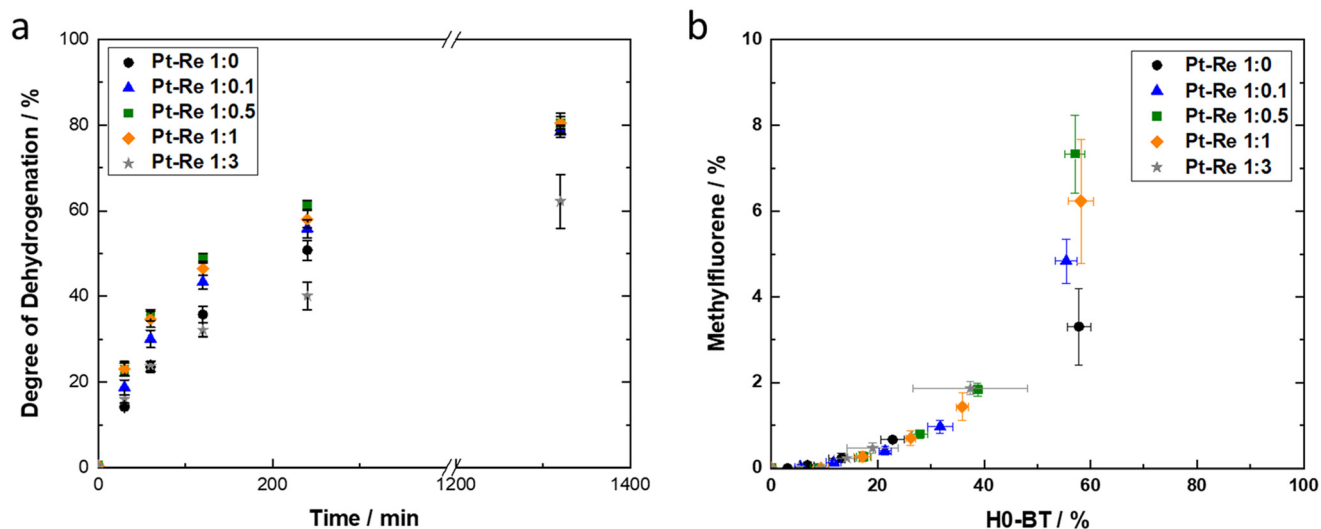| Sample	Pt–Cl/Å	CN (Cl)	Pt–Pt/Re/Å	CN (Pt/Re)	σ^2/Å^2 10^{-3}	δ_{E0}/eV	ρ/%
Pt foil	—	—	2.77 ± 0.01	12.0	2.8 ± 1.3	7.9 ± 1.0	1.0
Pt–Re 1:0	2.32 ± 0.08	0.7 ± 0.5	2.71 ± 0.03	6.0 ± 3.5	8.9 ± 5.6	6.9 ± 2.9	4.6
Pt–Re 1:0.1	2.20 ± 0.06	0.3 ± 0.2	2.69 ± 0.02	5.9 ± 1.6	9.9 ± 3.1	6.4 ± 1.4	1.6
Pt–Re 1:0.5	2.00 ± 0.09	0.3 ± 0.3	2.70 ± 0.03	6.1 ± 3.2	7.0 ± 5.1	2.9 ± 3.3	6.5
Pt–Re 1:1	2.01 ± 0.13	0.3 ± 0.4	2.68 ± 0.04	5.6 ± 1.8	7.0 (fixed)	3.1 ± 4.5	20.0
Pt–Re 1:3	2.05 ± 0.05	0.4 ± 0.2	2.68 ± 0.03	3.9 ± 1.7	7.6 ± 4.7	4.3 ± 2.6	5.2

Fig. 6 (a) Degree of dehydrogenation and (b) production of methylfluorene species during H$_2$ release from H12-BT. Reaction conditions: 250 °C, 1 atm, 0.0001 mol$_{Pt}$ mol$_{LOHC}$$^{-1}$, 31.01 g$_{H12-BT}$, 0.30 wt% Pt, 0–0.90 wt% Re, 1320 min, 0 mL$_{Ar}$ min^{-1}. Calculations according to eqn (5) based on GC-FID analysis of liquid samples, while error bars represent the standard deviation from three reproductions.

suppresses deep dehydrogenation to methylfluorene compounds even under long-term operation at harsh conditions.

The concept of selective sulphur-poisoning for enhancing the performance of catalysts for the dehydrogenation of hydrogen-rich, benzyltoluene-type LOHC systems was introduced by Auer et al., who demonstrated a suppressed side product formation during dehydrogenation of H18-DBT over monometallic Pt/Al$_2$O$_3$ catalysts.[8] This approach is intended to poison the most active sites, which are also the most attractive for sulphur poisoning. Some part of the activity is sacrificed to gain a higher selectivity towards H0-BT by suppressing the consecutive dehydrocyclisation

reaction. For nanoparticles, low coordinated kink and edge sites are assumed to show significant dehydrocyclisation activity.[8] Consequently, the herein prepared catalysts may provide a significantly increased fraction of highly active sites, which is typically linked to the morphology of the Pt nanoparticles. For example, the dehydrogenation of H18-DBT has been demonstrated to have a strong structural dependency in a study comparing Pt/Al$_2$O$_3$ catalysts with various well-defined Pt nanoparticle sizes in the range of 1.2–4.6 nm.[51] Here, the activity and the formation of methylfluorene species were the highest for 1.5 nm. As literature[12,19,20] and TPR results (Fig. 2) suggest strong interaction between the Re and Pt phase, the bimetallic
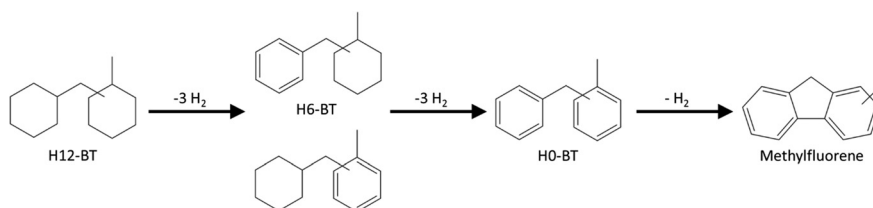

Fig. 7 Reaction scheme of the dehydrogenation of perhydro benzyltoluene including undesired "deep" dehydrogenation via the formation of methylfluorene species.

This journal is © The Royal Society of Chemistry 2024

Catal. Sci. Technol., 2024, **14**, 1775–1790 | 1783

catalysts may simply expose preferably coordinated Pt atoms to boost the dehydrogenation of H12-BT. This hypothesis is also supported by a decreasing coordination number of Pt in bimetallic Pt–Re catalysts according to EXAFS (Table 3). Here, the coordination of Pt in Pt–Re 1:3 is drastically decreased, which may explain the generally low activity due to the small Pt size. As already mentioned, limited desorption of H0-BT from most active sites may be at play as suggested for H0-DBT in the dehydrogenation of H18-DBT.[51]

As a selective size analysis of Pt nanoparticles is not feasible for the bimetallic catalysts (see above), the calculation of an initial turn-over frequency from the semi-batch experiments is not possible. This would directly link the proposed preferred morphology of Pt nanoparticles to the observed activity. However, an overall productivity of Pt in the various catalysts may be calculated to identify the most efficient catalyst. This productivity resembles a reaction rate, where the actual number of active sites is unknown, and is only based on the amount of Pt in the catalyst. Hence, the Re loading is not taken into account as it was previously shown to be inactive (Fig. S10†). As the Pt loading is comparable for all catalysts, the productivity follows a similar trend as the DoDH (Fig. 8). To obtain continuous data sampling for advanced kinetic analyses of the prepared catalysts, Ar was used as carrier gas for released H_2 by overflowing the LOHC during dehydrogenation even though technical H_2 release is done without a carrier gas. The productivity can then be calculated based on the concentration in the off-gas and the mass of Pt loaded with the catalyst according to eqn (3). The productivity spikes as soon as the catalyst is added at reaction temperature, which is then followed by an expected exponential decay of the productivity due to the semi-batch operation mode that leads to lower productivities with decreasing hydrogen-loading of the remaining LOHC

material in the reactor (Fig. 8a). Once again, the initial productivity of all bimetallic catalysts is increased drastically when compared to Pt/Al₂O₃. The twofold increase in productivity of Pt with the addition of half or equal amounts of Re in catalysts Pt–Re 1:0.5 and 1:1, respectively, strongly points toward a strong influence of Re on the physicochemical properties of Pt. Aside from the spike, the productivities are similar for Pt–Re 1:1 and 1:0.5. Hence, the present study focuses on the optimization and characterization of Pt–Re 1:0.5 for economic reasons. The strong productivity decay for Pt–Re 1:3, once again, suggests self-inhibiting mechanisms *via* desorption limitations.[51]

The addition of rhenium resulted in up to a twofold increase in maximum productivity of Pt for Pt–Re/Al₂O₃ catalysts (Fig. 8b), which may be linked to an optimized dispersion of Pt and electronic modification. To assess the strength of the interaction between the promoter and the active metal, a Pt–Re 1:0.5 catalyst and a Pt–Re 1:0 reference catalyst were reduced in H_2 at 250 and 700 °C in addition to the reduction at 400 °C applied as standard catalyst preparation procedure. Before catalytic testing, the reduced catalysts were analysed by means of STEM. Expectedly, the monometallic reference exhibits vast sintering resulting in large Pt nanoparticles with sizes larger than 6 nm (Fig. 9a) as reported in several studies.[52,53] Contrary, the previously identified mixed composition of nanoparticles, clusters, and single atoms in the bimetallic catalysts (Fig. 1) are observed for the Pt–Re 1:0.5 catalyst (Fig. 9b). The size distribution shifted only to a slightly larger range of 1.0–2.0 nm compared to 0.8–1.4 nm for the same catalyst after reduction at 400 °C (Fig. 1b). Hence, the Pt phase was significantly stabilized by the presence of Re allowing for elevated temperatures during reduction in H_2 without major sintering. This remarkable finding is explained by the strong bonding between rhenium
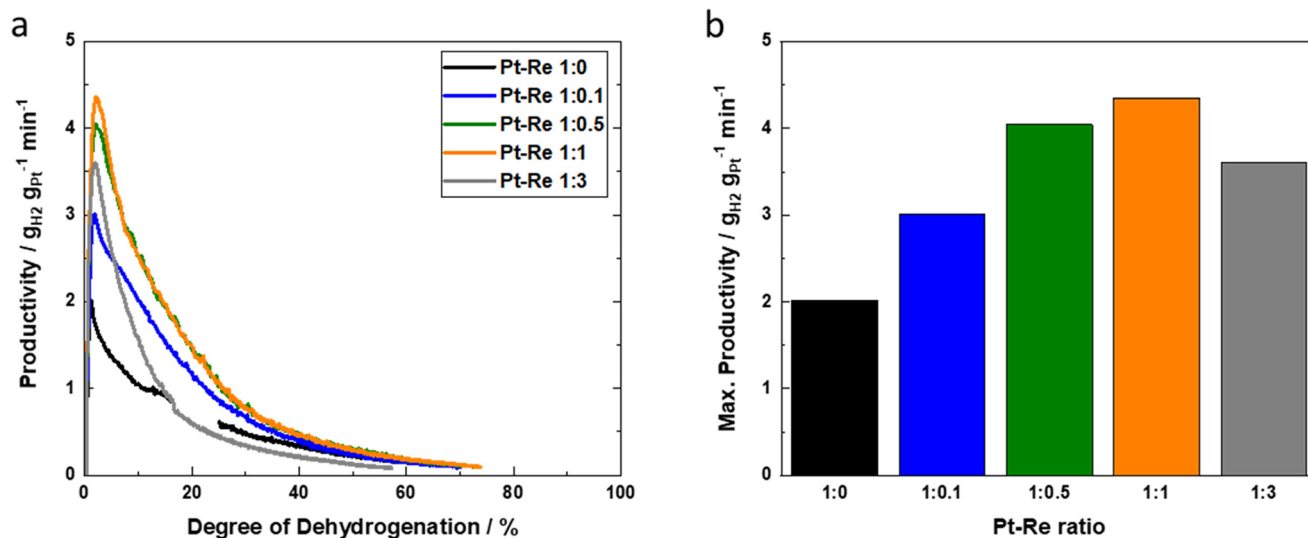

Fig. 8 (a) Productivity and (b) maximum productivity at low conversions during dehydrogenation of H12-BT. Reaction conditions: 250 °C, 1 atm, 0.0001 mol_{Pt} mol_{LOHC}^{-1}, 31.01 g_{H12-BT}, 0.30 wt% Pt, 0–0.90 wt% Re, 1320 min, 300 mL_{Ar} min^{-1}. Calculations according to eqn (3) based on TCD analysis of released H_2.

1784 | *Catal. Sci. Technol.*, 2024, **14**, 1775–1790

This journal is © The Royal Society of Chemistry 2024

and alumina, which in turn maintains the dispersion and stability of platinum.[20]

With the help of the presented results and literature, the several possibilities regarding the location of Re species in the catalyst may be discussed. Firstly, alloying of Pt and Re with high Pt content is suggested for small clusters by a density functional theory (DFT) study,[54] but could not be identified in the present studies. However, a certain contribution to the beneficial performance of Pt–Re/Al$_2$O$_3$ catalysts may be linked to low concentration of Re atoms in Pt clusters and nanoparticles. Secondly, Re species may simply modify the Al$_2$O$_3$ surface and enhance metal–support interaction with Pt. The superior stabilisation of clusters and nanoparticles during reduction of a bimetallic catalyst at elevated temperatures (Fig. 9b) supports this hypothesis. Further, the strong dependency of the Pt coordination number and consequentially the dispersion of Pt on the Re loading further hints towards such a dominating mode of Re promotion. Higher Re loadings seemingly induce a drastic increase in Pt dispersion resulting in small clusters with inferior specific activity.[51] As discussed, clear separation from electronic effects, which may play a minor role as well, is not possible. Such a combination of structural and electronic effects is also possible in a last possibility, where Re species enclose and stabilise Pt species, which is expected to efficiently suppress sintering. As no evidence for such co-location of different metal (oxide) species in the analysed clusters and nanoparticles is observed, we hypothesise surface modification of the support as the dominating beneficial effect in the herein presented catalysts.

To elucidate the importance of Pt nanoparticle stabilization during catalyst preparation, the monometallic and bimetallic catalysts were tested in the semi-batch dehydrogenation of H12-BT after reduction at different temperatures (Fig. 10). For both catalyst systems, a decelerated H$_2$ release was observed when increasing the reduction temperature from 400 to 700 °C. As expected from the presence of large nanoparticles according to STEM analysis (Fig. 9), the dehydrogenation rate of H12-BT using the monometallic Pt/Al$_2$O$_3$ catalyst after reduction at 700 °C was only half of the one obtained with the catalyst reduced at 400 °C. Also the Pt–Re/Al$_2$O$_3$ (Pt : Re ratio of 1 : 0.5) exhibits a lower activity after reduction at 700 °C compared to reduction at 400 °C. However, the relative loss in activity is smaller and the semi-batch dehydrogenation resembles the one using a monometallic catalyst after reduction at moderate temperatures. The catalysts were also reduced at 250 °C to assess potential effects. No change in activity was observed for Pt/Al$_2$O$_3$ compared to the reduction at 400 °C. Interestingly, the bimetallic catalyst exhibited a significantly lower activity after reduction at 250 °C compared to reduction at 400 °C. This observation strongly points towards beneficial electronic modification of Pt by Re when reducing at 400 °C. Such a modification is seemingly less pronounced or even absent for a reduction at 250 °C. While TPR analyses suggest major reduction of the oxidic precursor at 220 °C (Fig. 2), the ongoing reduction at increased temperatures may dominate electronic modification of Pt.

The dehydrogenation of H12-BT to H0-BT is a consecutive reaction via H6-BT isomers as intermediates (Fig. 7).[3] Comparison of the conversion of the reactant together with the lifetime and build-up of intermediates may therefore help to elucidate the effect of the bimetallic catalyst on the different reaction steps. An initial acceleration of the dehydrogenation has been observed for Pt–Re 1 : 0.5 compared to Pt–Re 1 : 0 (Fig. 6a), which is intrinsically linked to a rapid conversion of H12-BT
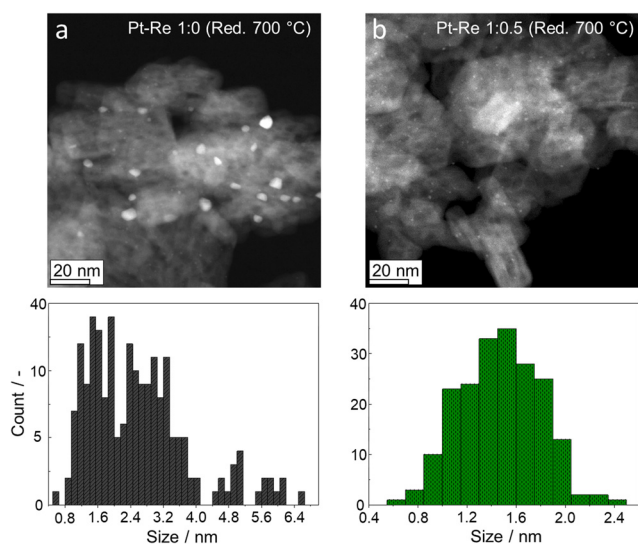

Fig. 9 High-angle annular dark field scanning transmission electron micrographs of (a) a monometallic Pt–Re 1 : 0 and (b) a bimetallic Pt–Re 1 : 0.5 after reduction at 700 °C for 120 min with histograms of the size distribution.
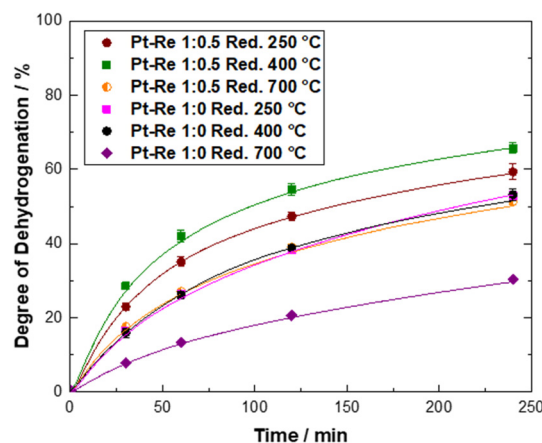

Fig. 10 Degree of dehydrogenation during H$_2$ release from H12-BT at 250 °C using monometallic Pt–Re 1 : 0 and bimetallic Pt–Re 1 : 0.5 catalysts after reduction at 250, 400, or 700 °C for 120 min. Reaction conditions: 250 °C, 1 atm, 0.0001 mol$_{Pt}$ mol$_{LOHC}^{-1}$, 31.01 g$_{H12\text{-}BT}$, 0.30 wt% Pt, 0 or 0.15 wt% Re, 240 min, 300 mL$_{Ar}$ min^{-1}. Calculations for symbols according to eqn (5) are based on GC-FID analysis of liquid samples, while the solid lines are obtained according to eqn (2) based on TCD analysis of released H$_2$.
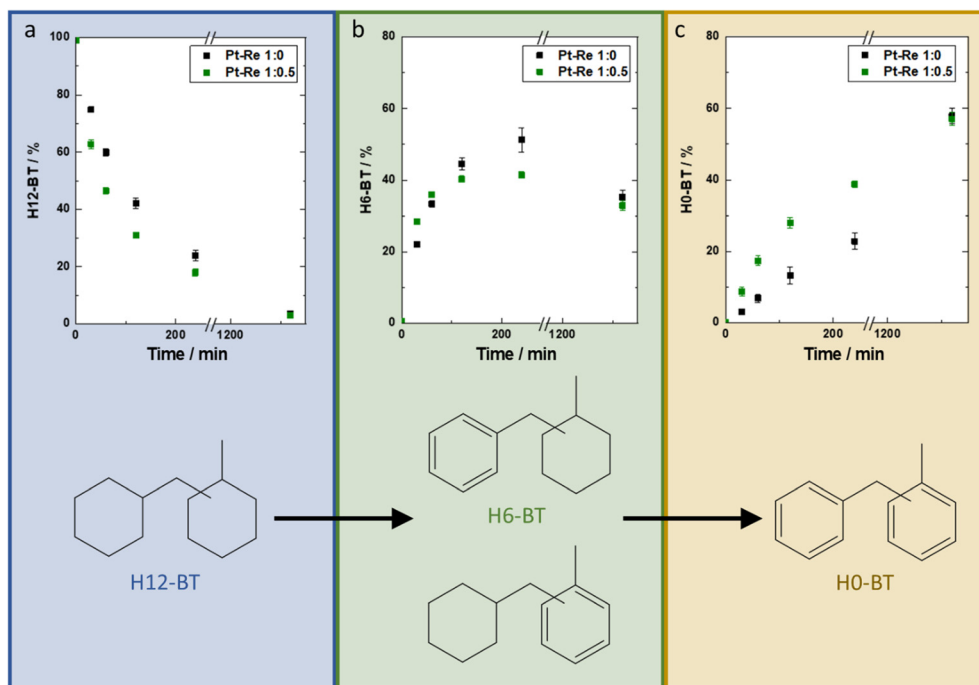
This journal is © The Royal Society of Chemistry 2024

Catal. Sci. Technol., 2024, **14**, 1775–1790 | 1785

Fig. 11 (a) Fraction of H12-BT and (b) build-up of formed H6-BT as well as (c) H0-BT during H$_2$ release from H12-BT using monometallic Pt–Re 1 : 0 and bimetallic Pt–Re 1 : 0.5 catalysts together with the reaction sequence of the dehydrogenation. Reaction conditions: 250 °C, 1 atm, 0.0001 mol$_{Pt}$ mol$_{LOHC}^{-1}$, 31.01 g$_{H12-BT}$, 0.30 wt% Pt, 0 or 0.15 wt% Re, 1320 min, 300 mL$_{Ar}$ min^{-1}.

(Fig. 11a). However, the accelerated H$_2$ release also originates from an accelerated dehydrogenation of H6-BT (Fig. 11b). This is indicated by a less pronounced build-up of H6-BT over time due to faster formation of the final product H0-BT (Fig. 11c). Consequentially, Pt–Re/Al$_2$O$_3$ may also be an efficient catalyst for the rapid dehydrogenation of H6-BT intermediates. This relationship can be visualized when comparing the build-up of H6-BT intermediates with the molar fractions of the reactant H12-BT and product H0-BT (Fig. S11†) or simply as a function of the DoDH

(Fig. 12). For Pt–Re 1 : 0.5, the maximum measured molar fraction of H6-BT species is 42%, while Pt–Re 1 : 0 accumulates up to 51% during dehydrogenation of H12-BT at 250 °C. This accelerated dehydrogenation of Hx-BT species is expected to be relevant for all isomers. However, the present data using commercially relevant isomeric mixture of technical H12-BT does not allow to draw conclusions as the *para* H12-BT isomer has been identified to allow for fastest dehydrogenation using Pt/Al$_2$O$_3$ catalysts in a study by Park, Suh *et al.*[4] A detailed study using isolated or enriched isomers of H12-BT for testing the dehydrogenation with the herein developed Pt–Re/Al$_2$O$_3$ catalysts would be required.

These observations suggest an efficient dehydrogenation of H12-BT over Pt–Re catalysts due to rapid initial conversion of H12-BT and, more important, a shorter lifetime of H6-BT species. A facilitated desorption of H0-BT may also explain the enhanced overall activity, while the observed enhanced formation of methylfluorene species suggests strong binding of H0-BT on a significant fraction of the active sites. All of the listed reaction steps directly depend on the surface composition of Pt nanoparticles and hence may be directly linked to physical and electronic Pt–Re interaction.[35,36] Physical modification of Pt by rhenium promotion is indicated by smaller coordination numbers in bimetallic catalysts when compared to Pt/Al$_2$O$_3$ (Table 3) and simply provides an increased dispersion of Pt. More importantly, the share of low-coordinated sites may be altered affecting intrinsic dehydrogenation activity of the Pt surface. The accelerated dehydrogenation of H6-BT species may be linked
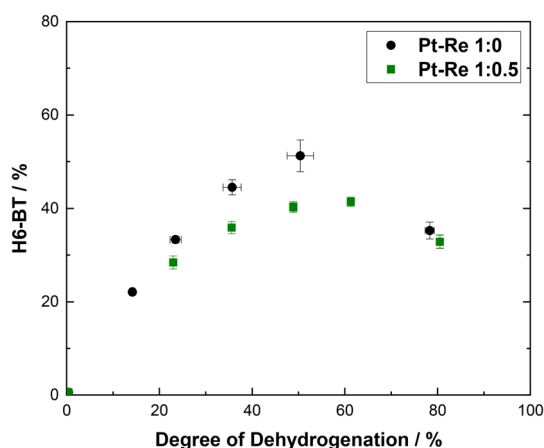

Fig. 12 Relationship between the concentration of H6-BT and the degree of dehydrogenation during H$_2$ release from H12-BT using monometallic Pt–Re 1 : 0 and bimetallic Pt–Re 1 : 0.5 catalysts. Reaction conditions: 250 °C, 1 atm, 0.0001 mol$_{Pt}$ mol$_{LOHC}^{-1}$, 31.01 g$_{H12-BT}$, 0.30 wt% Pt, 0 or 0.15 wt% Re, 1320 min, 300 mL$_{Ar}$ min^{-1}.

to such a modification. Enhanced H0-BT adsorption has been observed in monometallic Pt catalysts for certain nanoparticle sizes, which results in an enhanced formation of methylfluorene[51] similar to the observations in the present study. This may also explain the less enhanced activity of Pt–Re catalysts at higher DoDHs as some active sites may be blocked by H0-BT and/or methylfluorene species. Either way, selective poisoning with sulphur has been demonstrated to suppress side product formation from limited desorption of the desired dehydrogenated LOHC.[3,8]

Lastly, the dehydrogenation of H12-BT was compared for Pt–Re 1:0 and Pt–Re 1:0.5 at various reaction temperatures in the range of 210 to 250 °C. The previously identified accelerated initial dehydrogenation when using bimetallic Pt–Re catalysts (Fig. 6a) was also observed for lower reaction temperatures (Fig. 13a). In-line with the discussion above, the hydrogen release rate in the time range 120–240 min was comparable or even faster (see 240 °C) for the monometallic catalyst. However, the overall dehydrogenation was superior at all temperatures for the bimetallic catalyst due to the strong activation effects in the first 120 min of reaction. Side products were detected independent from the dehydrogenation temperatures (Fig. S12†). The side product formation was, once again, increased for Pt–Re/Al$_2$O$_3$ catalysts, which strongly supports the hypothesized structural changes of Pt due to rhenium promotion. The obtained productivities (Fig. S13†) were compared in an Arrhenius plot (Fig. 13b) resulting in apparent activation energies of −182.2 and −170.5 kJ mol^{-1} for Pt–Re 1:0 and Pt–Re 1:0.5, respectively. These values are in-line with reported activation energies from the literature for H18-DBT dehydrogenation using a commercial Pt-based dehydrogenation catalyst.[55]

Summary and conclusions

Herein, a bimetallic Pt–Re/Al$_2$O$_3$ catalyst, prepared *via* wet impregnation with strong ion adsorption, was developed for the dehydrogenation of H12-BT in the context of H$_2$ release from the technically highly relevant H0-BT/H12-BT LOHC system. Optimization of the Re loading resulted in a more than two-fold increase in initial productivity of Pt when compared to a monometallic Pt/Al$_2$O$_3$ reference. The optimum gravimetric Pt–Re ratios for 0.3 wt% Pt catalysts have been found at 1:1 or 1:0.5, while already a 1:0.1 ratio enabled a significant increased productivity. Only high Re loadings with a Pt–Re ratio of 1:3 resulted in a detrimental performance, which may be due to a low general accessibility of Pt with these high Re loadings TPRs of the calcined catalysts indicate full reduction of Pt and partial reduction of rhenium oxide.

Our results suggest that the structural modification of Pt by rhenium results in higher dispersion of Pt. The dispersion was successfully analysed by means of XAS as common characterization techniques, such as chemisorption or EDX, are not suitable to distinguish between the elements in the given catalyst materials with low metal loadings. EXAFS analyses after *in situ* reduction suggest a strongly decreasing coordination number of Pt with increasing Re loading. While the coordination of Pt may be optimal for Pt–Re ratios of 1:1 and 1:0.5, the low coordination number of Pt at a ratio of 1:3 may suppress efficient catalysis. The lowered Pt coordination number in bimetallic catalysts may be a result of smaller nanoparticles or an altered geometry of Pt as the active phase. In addition, modification of the catalysts with Re was found to drastically increase the thermal stability of the Pt phase. The bimetallic catalyst suffered only from
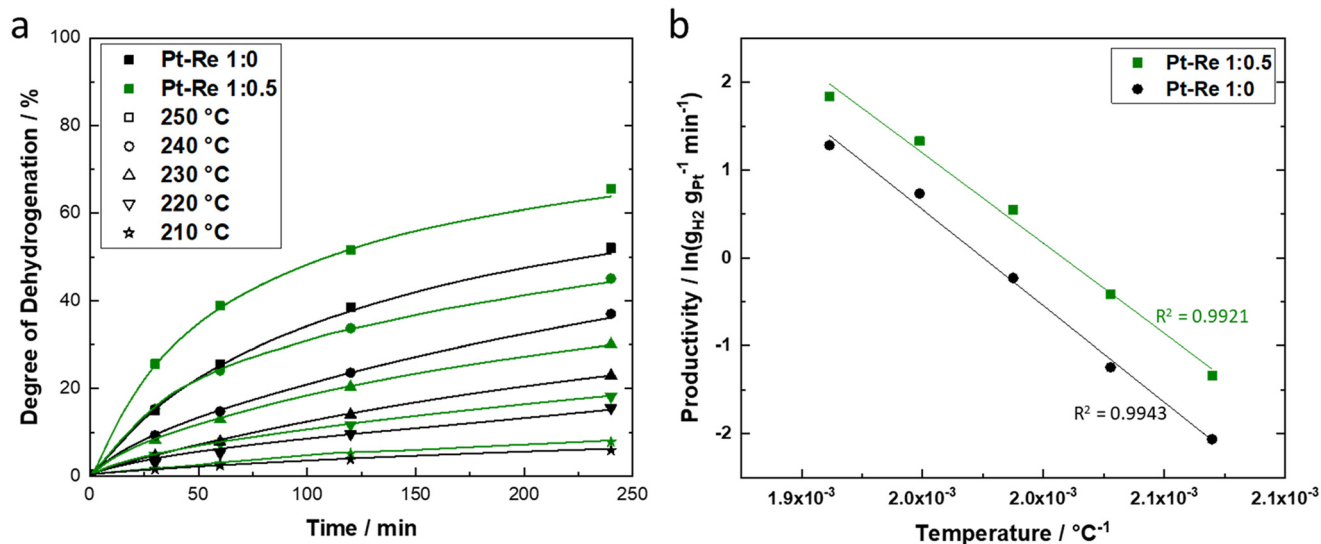

Fig. 13 Degree of dehydrogenation during H$_2$ release from H12-BT at various temperatures using monometallic Pt–Re 1:0 and bimetallic Pt–Re 1:0.5 catalysts (a) together with an Arrhenius plot comparing the productivity at 5% DoDH (b). Reaction conditions: 210–250 °C, 1 atm, 0.0001 mol$_{Pt}$ mol$_{LOHC}$$^{-1}$, 31.01 g$_{H12-BT}$, 0.30 wt% Pt, 0 or 0.15 wt% Re, 240 min, 300 mL$_{Ar}$ min^{-1}. Calculations for symbols according to eqn (5) are based on GC-FID analysis of liquid samples, while the solid lines are obtained according to eqn (2) based on TCD analysis of released H$_2$.

minor sintering during reduction at 700 °C resulting in a comparable catalyst activity in the dehydrogenation of H12-BT when compared to catalyst activation at 400 °C. In contrast, nanoparticles >5 nm were identified by means of STEM for a monometallic Pt/Al$_2$O$_3$ catalyst after reduction at 700 °C, which consequentially lead to a strongly reduced activity. This high resistance against harsh conditions during catalyst preparation and operation may facilitate technical use of these bimetallic catalyst as hot-spots or deviations from desired process conditions may not harm the bimetallic catalyst in the same manner as its more sensitive monometallic counterpart. Aside from this so-called ensemble effect, the presence of Re most likely also introduces electronic modification of Pt as observed from XANES.

Analysis of the reaction network of the dehydrogenation of H12-BT to H0-BT *via* H6-BT species suggests a shortened lifetime of the H6-BT intermediates for Pt–Re/Al$_2$O$_3$ catalysts. "Deep" dehydrogenation of H0-BT to methylfluorene species, an undesired side-reaction due to the high melting points of methylfluorenes, is more pronounced with the bimetallic Pt–Re catalyst compared to the monometallic Pt/Al$_2$O$_3$ catalyst. This enhanced side product formation may become critical for technical applications at a DoDH >40%. Methylfluorene formation is a consequence of a stronger adsorption of H0-BT to the active sites of the bimetallic catalyst. The resulting, temporary blocking of active sites by H0-BT and methylfluorene is the reason why positive effects of the bimetallic catalyst on activity are mainly seen for short reaction times, low DoDHs and low contents of H0-BT in the reaction mixture.

Overall, a promising catalyst system for the dehydrogenation of H12-BT has been developed, which now requires further optimization to become a suitable candidate for technical application. In particular, methylfluorene formation must be suppressed *via* an enhanced H0-BT desorption. Both effects can be addressed by selective sulphur poisoning and such dedicated poisoning studies are ongoing in our laboratories. A further, very attractive technical option to make use of the here reported results is to combine a Pt–Re/Al$_2$O$_3$ and a Pt/Al$_2$O$_3$ catalyst in a layered fixed-bed or in a two-step dehydrogenation process. In this way, the bimetallic catalyst can provide its superior dehydrogenation performance at low DoDH, while the monometallic catalyst can serve for the further hydrogen release to realize high DoDHs and the desired maximum hydrogen yield for the overall process.

Author contributions

DS: conceptualization; investigation, data curation & formal analysis (catalyst preparation & activation, catalyst testing, PZC, TPR); formal analysis (HAADF-STEM); visualization; writing – original draft. PiW: investigation (catalyst preparation & activation, catalyst testing). BBS: investigation, data curation, formal analysis & visualization (XAS); writing –

review & editing. AK: investigation (HAADF-STEM, STEM-EDX). EH: investigation, data curation & formal analysis, (PZC, XRD). PaW: investigation (hydrogenation of H0-BT). AZ: investigation (XAS). AH: investigation, data curation & supervision (HAADF-STEM, STEM-EDX), writing – review & editing. DED: investigation, data curation, formal analysis, supervision & visualization (XAS); writing – review & editing. JDG: resources & supervision (XAS); validation; writing – review & editing. PeW: conceptualization; funding acquisition; project administration; resources; validation; writing – review & editing. MW: conceptualization; funding acquisition; project administration; resources; validation; visualization; writing – original draft.

Conflicts of interest

PW is co-founder and minority shareholder of Hydrogenious LOHC Technologies GmbH, Erlangen, a company that has commercialized equipment for hydrogen storage using the LOHC technology.

Acknowledgements

References

1 P. Preuster, C. Papp and P. Wasserscheid, Liquid Organic Hydrogen Carriers (LOHCs): Toward a Hydrogen-free Hydrogen Economy, *Acc. Chem. Res.*, 2017, **50**, 74.

2 D. Teichmann, W. Arlt, P. Wasserscheid and R. Freymann, A future energy supply based on Liquid Organic Hydrogen Carriers (LOHC), *Energy Environ. Sci.*, 2011, **4**, 2767.

3 T. Rüde, S. Dürr, P. Preuster, M. Wolf and P. Wasserscheid, Benzyltoluene/perhydro benzyltoluene – pushing the performance limits of pure hydrocarbon liquid organic hydrogen carrier (LOHC) systems, *Sustainable Energy Fuels*, 2022, **6**, 1541.

4 T. W. Kim, Y. Jo, K. Jeong, H. Yook, J. W. Han, J. H. Jang, G. B. Han, J. H. Park and Y.-W. Suh, Tuning the isomer

1788 | *Catal. Sci. Technol.*, 2024, **14**, 1775–1790

This journal is © The Royal Society of Chemistry 2024

composition is a key to overcome the performance limits of commercial benzyltoluene as liquid organic hydrogen carrier, *J. Energy Storage*, 2023, **60**, 106676.

5 M. Amende, C. Gleichweit, K. Werner, S. Schernich, W. Zhao, M. P. A. Lorenz, O. Höfert, C. Papp, M. Koch, P. Wasserscheid, M. Laurin, H.-P. Steinrück and J. Libuda, Model Catalytic Studies of Liquid Organic Hydrogen Carriers: Dehydrogenation and Decomposition Mechanisms of Dodecahydro-N-ethylcarbazole on Pt(111), *ACS Catal.*, 2014, **4**, 657.

6 A. Leinweber and K. Müller, Hydrogenation of the Liquid Organic Hydrogen Carrier Compound Monobenzyl Toluene: Reaction Pathway and Kinetic Effects, *Energy Technol.*, 2018, **6**, 513.

7 N. Szesni, F. Frankl, S. Sturm, P. Wasserscheid, A. Seidel and A. Boesmann, Platinum-sulfur-based shell catalyst, production and use thereof in the dehydrogenation of hydrocarbons, US20210077984A1, 2021.

8 F. Auer, D. Blaumeiser, T. Bauer, A. Bösmann, N. Szesni, J. Libuda and P. Wasserscheid, Boosting the activity of hydrogen release from liquid organic hydrogen carrier systems by sulfur-additives to Pt on alumina catalysts, *Catal. Sci. Technol.*, 2019, **9**, 3537.

9 E. Herzinger and M. Wolf, Perspectives and Potential of Liquid Organic Hydrogen Carriers in the German Energy Scenario, *Chem. Ing. Tech.*, 2023, **96**(1–2), 65–73.

10 A. Hoppe, Landesregierung fördert Aufbau einer weltweit einzigartigen Speicher- und Transporttechnologie für Wasserstoff mit neun Millionen Euro, **https://www.klimaschutz.nrw.de/aktuelles/detail/landesregierung-foerdert-aufbau-einer-weltweit-einzigartigen-speicher-und-transporttechnologie-fuer-wasserstoff-mit-neun-millionen-euro**, (accessed 5 October 2022).

11 S. Riepe, Wasserstofftankstelle Erlangen geht im Rahmen der #WDWS2022 in den Betrieb, **https://h2.live/news/2453/**, (accessed 5 October 2022).

12 H. E. Kluksdahl, Reforming a sulfur-free naphtha with a platinum-rhenium catalyst, US3415737A, 1966.

13 K. Jothimurugesan, S. Bhatia and R. D. Srivastava, Kinetics of dehydrogenation of methylcyclohexane over a platinum-rhenium-alumina catalyst in the presence of added hydrogen, *Ind. Eng. Chem. Fundam.*, 1985, **24**, 433.

14 P. A. van Trimpont, G. B. Marin and G. F. Froment, Kinetics of methylcyclohexane dehydrogenation on sulfided commercial platinum/alumina and platinum-rhenium/alumina catalysts, *Ind. Eng. Chem. Fundam.*, 1986, **25**, 544.

15 P. G. Menon and Z. Paál, Some Aspects of the Mechanisms of Catalytic Reforming Reactions, *Ind. Eng. Chem. Res.*, 1997, **36**, 3282.

16 M. Pacheco, Reaction kinetics of methylcyclohexane dehydrogenation over a sulfided Pt + Re/Al$_2$O$_3$ reforming catalyst, *J. Catal.*, 1985, **96**, 507.

17 F. Alhumaidan, D. Tsakiris, D. Cresswell and A. Garforth, Hydrogen storage in liquid organic hydride: Selectivity of MCH dehydrogenation over monometallic and bimetallic Pt catalysts, *Int. J. Hydrogen Energy*, 2013, **38**, 14010.

18 V. Shum, The effects of rhenium and sulfur on the maintenance of activity and selectivity of platinum/alumina hydrocarbon conversion catalysts II. Experiments at elevated pressure, *J. Catal.*, 1986, **99**, 126.

19 F. H. Ribeiro, A. L. Bonivardi, C. Kim and G. A. Somorjai, Transformation of Platinum into a Stable, High-Temperature, Dehydrogenation-Hydrogenation Catalyst by Ensemble Size Reduction with Rhenium and Sulfur, *J. Catal.*, 1994, **150**, 186.

20 Y. Yermakov and B. N. Kuznetsov, Supported metallic catalysts prepared by decomposition of surface ornagometallic complexes, *J. Mol. Catal.*, 1980, **9**, 13.

21 F. Alhumaidan, D. Cresswell and A. Garforth, Hydrogen Storage in Liquid Organic Hydride: Producing Hydrogen Catalytically from Methylcyclohexane, *Energy Fuels*, 2011, **25**, 4217.

22 S. Mustafa, B. Dilara, K. Nargis, A. Naeem and P. Shahida, Surface properties of the mixed oxides of iron and silica, *Colloids Surf., A*, 2002, **205**, 273.

23 E. N. Bakatula, D. Richard, C. M. Neculita and G. J. Zagury, Determination of point of zero charge of natural organic materials, *Environ. Sci. Pollut. Res.*, 2018, **25**, 7823.

24 C. A. Schneider, W. S. Rasband and K. W. Eliceiri, NIH Image to ImageJ: 25 years of image analysis, *Nat. Methods*, 2012, **9**, 671.

25 B. Ravel and M. Newville, ATHENA, ARTEMIS, HEPHAESTUS: data analysis for X-ray absorption spectroscopy using IFEFFIT, *J. Synchrotron Radiat.*, 2005, **12**, 537.

26 N. Brückner, K. Obesser, A. Bösmann, D. Teichmann, W. Arlt, J. Dungs and P. Wasserscheid, Evaluation of industrially applied heat-transfer fluids as liquid organic hydrogen carrier systems, *ChemSusChem*, 2014, **7**, 229.

27 S. Augustine, On the mechanism for the platinum-catalyzed reduction of rhenium in PtRe/γ-Al$_2$O$_3$, *J. Catal.*, 1989, **116**, 184.

28 B. Isaacs, The effect of drying temperature on the temperature-programmed reduction profile of a platinum/rhenium/alumina catalyst, *J. Catal.*, 1982, **77**, 43.

29 R. Prestvik, K. Moljord, K. Grande and A. Holmen, The Influence of Pretreatment on the Metal Function of a Commercial Pt–Re/Al$_2$O$_3$ Catalyst, *J. Catal.*, 1998, **174**, 119.

30 Y. Guryev, I. I. Ivanova, V. V. Lunin, W. Grünert and M. van den Berg, Characterization of metal segregation in Pt–Re/Al$_2$O$_3$ reforming catalysts, *Appl. Catal., A*, 2007, **329**, 16.

31 R. Mieville, Platinum-rhenium interaction: A temperature-programmed reduction study, *J. Catal.*, 1984, **87**, 437.

32 F. Hilbrig, C. Michel and G. L. Haller, A XANES-TPR study of platinum-rhenium/alumina catalysts, *J. Phys. Chem.*, 1992, **96**, 9893.

33 L. Y. Chen, Y. Q. Ni, J. L. Zang, L. W. Lin, X. H. Luo and S. Cheng, Structure Characterization of Platinum/Alumina, Rhenium/Alumina, and Platinum-Rhenium/Alumina Catalysts, *J. Catal.*, 1994, **145**, 132.

34 P. Malet, Effect of chlorine in the formation of PtRe alloys in PtRe/Al$_2$O$_3$ catalysts, *J. Catal.*, 1989, **115**, 567.

35 W. Sachtler and R. A. van Santen, in *Advances in Catalysis*, Elsevier, 1977, pp. 69–119.

This journal is © The Royal Society of Chemistry 2024

Catal. Sci. Technol., 2024, **14**, 1775–1790 | **1789**

36 J. P. Bosco, M. P. Humbert and J. G. Chen, in *Design of Heterogeneous Catalysts*, ed. U. S. Ozkan, Wiley-VCH, Weinheim, 2009, pp. 195–212.

37 J.-D. Grunwaldt, M. Caravati, S. Hannemann and A. Baiker, X-ray absorption spectroscopy under reaction conditions: suitability of different reaction cells for combined catalyst characterization and time-resolved studies, *Phys. Chem. Chem. Phys.*, 2004, **6**, 3037.

38 E. Welter, R. Chernikov, M. Herrmann and R. Nemausat, A beamline for bulk sample x-ray absorption spectroscopy at the high brilliance storage ring PETRA III, *AIP Conf. Proc.*, 2019, **2054**, 40002.

39 M. Rønning, T. Gjervan, R. Prestvik, D. G. Nicholson and A. Holmen, Influence of Pretreatment Temperature on the Bimetallic Interactions in Pt-Re/Al2O3 Reforming Catalysts Studied by X-Ray Absorption Spectroscopy, *J. Catal.*, 2001, **204**, 292.

40 L. DeRita, J. Resasco, S. Dai, A. Boubnov, H. V. Thang, A. S. Hoffman, I. Ro, G. W. Graham, S. R. Bare, G. Pacchioni, X. Pan and P. Christopher, Structural evolution of atomically dispersed Pt catalysts dictates reactivity, *Nat. Mater.*, 2019, **18**, 746.

41 J. Resasco, L. DeRita, S. Dai, J. P. Chada, M. Xu, X. Yan, J. Finzel, S. Hanukovich, A. S. Hoffman, G. W. Graham, S. R. Bare, X. Pan and P. Christopher, Uniformity Is Key in Defining Structure-Function Relationships for Atomically Dispersed Metal Catalysts: The Case of Pt/CeO$_2$, *J. Am. Chem. Soc.*, 2020, **142**, 169.

42 P. Kuang, Y. Wang, B. Zhu, F. Xia, C.-W. Tung, J. Wu, H. M. Chen and J. Yu, Pt Single Atoms Supported on N-Doped Mesoporous Hollow Carbon Spheres with Enhanced Electrocatalytic H2-Evolution Activity, *Adv. Mater.*, 2021, **33**, e2008599.

43 C.-C. Hung, C.-Y. Yeh, C.-C. Shih and J.-R. Chang, Oxychlorination Redispersion of Pt Catalysts: Surface Species and Pt-support Interactions Characterized by X-Ray Absorption and FT-IR Spectroscopy, *Catalysts*, 2019, **9**, 362.

44 J. Barbier, Reduction of Pt/Al$_2$O$_3$ catalysts: Effect of hydrogen and of water and hydrochloric acid vapor on the accessibility of platinum, *J. Catal.*, 1992, **137**, 377.

45 J. F. Lambert, E. Marceau, B. Shelimov, J. Lehman, V. Le Bel de Penguilly, X. Carrier, S. Boujday, H. Pernot and M. Che, in *12th International Congress on Catalysis, Proceedings of the 12th ICC*, Elsevier, 2000, pp. 1043–1048.

46 D. Bazin and J. J. Rehr, Comment on "Operando DRIFTS and XANES Study of Deactivating Effect of CO$_2$ on a Ce$_{0.8}$Cu$_{0.2}$O$_2$ CO-PROX Catalyst", *J. Phys. Chem. C*, 2011, **115**, 23233.

47 H. Yao, Surface interactions in the system Re/γ-Al$_2$O$_3$, *J. Catal.*, 1976, **44**, 392.

48 A. Tougerti, S. Cristol, E. Berrier, V. Briois, C. La Fontaine, F. Villain and Y. Joly, XANES study of rhenium oxide compounds at the L1 and L3 absorption edges, *Phys. Rev. B: Condens. Matter Mater. Phys.*, 2012, **85**, 125136.

49 Y. Takahashi, T. Uruga, K. Suzuki, H. Tanida, Y. Terada and K. H. Hattori, An atomic level study of rhenium and radiogenic osmium in molybdenite, *Geochim. Cosmochim. Acta*, 2007, **71**, 5180.

50 P. Meriaudeau, J. F. Dutel, M. Dufaux and C. Naccache, in *Metal-Support and Metal-Additive Effects in Catalysis, Proceedings of an International Symposium organized by the Institut de Recherches sur la Catalyse — CNRS — Villeurbanne and sponsored by the Centre National de la Recherche Scientifique*, Elsevier, 1982, pp. 95–104.

51 F. Auer, A. Hupfer, A. Bösmann, N. Szesni and P. Wasserscheidpeter, Influence of the nanoparticle size on hydrogen release and side product formation in liquid organic hydrogen carrier systems with supported platinum catalysts, *Catal. Sci. Technol.*, 2020, **10**, 6669.

52 Z. Liu, X. Li, Z. Chen, P. Ying, Z. Feng and C. Li, Effect of reduction method on the surface states of Pt/Al$_2$O$_3$, *J. Fuel Chem. Technol.*, 2009, **37**, 205.

53 W. Yu, M. D. Porosoff and J. G. Chen, Review of Pt-based bimetallic catalysis: from model surfaces to supported catalysts, *Chem. Rev.*, 2012, **112**, 5780.

54 L. E. Gálvez-González, A. Posada-Amarillas and L. O. Paz-Borbón, Structure, Energetics, and Thermal Behavior of Bimetallic Re-Pt Clusters, *J. Phys. Chem. A*, 2021, **125**, 4294.

55 S. Park, M. Naseem and S. Lee, Experimental Assessment of Perhydro-Dibenzyltoluene Dehydrogenation Reaction Kinetics in a Continuous Flow System for Stable Hydrogen Supply, *Materials*, 2021, **14**, 7613.

1790 | *Catal. Sci. Technol.*, 2024, **14**, 1775–1790

This journal is © The Royal Society of Chemistry 2024